DEFORMATIONS, FORCES, AND STRESS FORMATIONS ANALYSIS IN SLIDING CONTACT BETWEEN A RIGID/HARD CYLINDER ON AN ELASTIC-PLASTIC CYLINDER

Rifky Ismail[1)], M. Tauviqirrahman[2)], Jamari[2)], Berkah Fajar T.K.[2)], and D.J. Schipper[1)]
1) Laboratory for Surface Technology and Tribology, Faculty of Engineering Technology, University of Twente, P.O. Box 217 7500 AE Enshede, The Netherlands
2) Department of Mechanical Engineering, University of Diponegoro, Semarang
Address: Jl. Prof. Sudharto, UNDIP Tembalang Phone: 024-7460059 ext. 104
E mail : rifky_mec@yahoo.com[1)]

ABSTRACT

This work presents the results of a finite element analysis (FEA) which is used to simulate two-dimensional (2D) sliding between a rigid/hard cylinder on an elastic-plastic cylinder. The material for the top cylinder is modeled as rigid, and the bottom cylinder is modeled as elastic-plastic and follows the von Mises yield criterion. The finite element software, ANSYS, is used to analyze the deformations, reaction forces, and stresses on the lower cylinder. The mesh was refined in the contacting area in order to achieve the convergence. The FEA provides trends in the deformations, reaction forces, and stresses as a function of the interferences and sliding distance between the cylinders. Results are presented for both frictionless and frictional sliding and comparisons are drawn. The formation and distribution of stresses along the sliding distance are presented in von Mises stress contour plot. Result show that for the plastic loading case the ratio of the horizontal force to the vertical reaction force is zero at the point where the cylinders are perfectly aligned about the vertical axis. The loading and unloading phenomena between two interfering cylinder is performed.

Keyword: Finite element analysis, sliding contact, line contact, elastic-plastic.

INTRODUCTION

This work presents the results of a finite element analysis (FEA) which is used to simulate two-dimensional (2D) sliding between a rigid/hard cylinder on an elastic-plastic cylinder. In the mechanical engineering application, the sliding contact results wear of the component. The wear phenomena control the component life time. The good wear prediction will prevent the mechanical component cycle fall into a severe condition [1]. The severe wear result in rough deeply torn surfaces much rougher than the original surface [2]. This circumstance can be followed by the failure of the mechanical component if there is no preventive action .

The solid-to-solid contact between the surfaces is made at their surface asperities. When two rough surfaces slide across one another, primarily the asperities on the surface will be in contact. The asperities of the surfaces often slide in difference interferences and result different friction, wear, and residual deformation in the contacting surface. In the micro scale, these asperity contacts often play a significant role in the tribological performance of mechanical systems.

Over the years, many researchers have conducted some study analytically dealing with elastic and elasticplastic contact. Early works based on this idea were published by Abbot and Firestone [3] for pure plastic asperity response and by Greenwood and Williamson [4] for purely elastic contact. Some results were published in order to extend the Greenwood and Williamson model in the elastic regime to a variety of geometries and different basic assumptions [5-9]. Normal spherical contacts are considered in the elastic-plastic regime by Evseev et al. [10], Chang et al. [11], and Zhao et al. [12].

A widely accepted model of rough surface topography based on the idea of multitude asperities, which may have various forms of their summits, e.g. hemispherical, elliptic or parabolic. Recently, the new model based on elliptical asperity contact has been proposed by Jamari [13, 14, 15]. Jamari has been proposed an elastic-plastic contact model which has been validated experimentally and showed an excellent agreement between the model and experiment.

Finite element method (FEM) is another tools to solve the contact problem. Most commercial software

packages provide a large number of options, including coefficient of friction, contact condition, and material properties to solve the simulation [16]. Vu-Quoc et al. [17] have been used FEA to analyze normal contact between two spheres, which by symmetry is equivalent to that of one sphere in contact with a rigid flat. Adams and Nosonovsky [18] provide a review of contact modeling with an emphasis on the forces of contact and their relationship to the geometrical, material, and mechanical properties of the contacting bodies. Recently, Jackson and Green [19], Wang and Keer [20], and Nelias et al. [21], have explored hemispherical elastic-plastic contact in a normal loading situation.

In FEA of sliding contact, Faulkner and Arnell [22] observed sliding contact between two hemispheres in 3D model [23]. This research is continued by Jackson et al [24] and Moody [23]. Vijaywargiya and Green [25] has studied 2D sliding contact simulation between two elastic-perfectly plastic cylinder. This work is continuing 2D sliding contact between two cylinders. The difference between the present study and the previous work is the upper asperity is set to be hard / rigid. The rigid assumption is chosen in order to describe the condition where a counter face part has much higher modulus of elasticity than the main body. The high modulus elasticity material, i.e. carbide, in some cases slide over a softer material. This model can be applied in analyzing that case. Another advantage of this model is able to shorten the simulation time.

METHODOLOGY

Finite element method was constructed using the commercial software ANSYS Version 9.0. FEM model were assembled of two plane semi-circles representing the sliding cylinders. The solid part of the model, Fig. 1 used two-dimensional structural solid elements, designated as PLANE82 in ANSYS. The model consists of 25,000 nodes and 8,455 elements. Contact between cylinders was simulated using the quadratic surface-to-surface contact element TARGE169 and CONTA172 at the interfaces. Once the predetermined regions are established, ANSYS is used to automatically mesh the said regions. The properties of the cylinders a used in the simulations are given in Table 1.

To simplify the problem, there are some assumptions that are used:

1. In the direction perpendicular to sliding, the bottom cylinder is considered to be infinitely long. This enables the FE model to be in 2D under the assumption of plane strain behaviour.
2. The sliding bodies are idealized to have elastic-plastic with strain hardening behaviour.
3. Sliding is simulated as a quasi-static process while time-dependent phenomena are not analyzed.
4. Temperature effects that occur due to sliding are not considered, and the material properties used are assumed to be at room temperature.

Table 1. Cylinders properties

	Bottom cylinder	Top cylinder
Elastic modulus (GPa)	68.9	Rigid
Poisson's ratio	0.330	
Geometry (mm)	Radius = 1000	Radius = 1000

The critical vertical interference, ω_c was derived by Green [26] for cylindrical contact and it is employed now. This quantity is derived by using the distortion energy yield criterion at the site of maximum von Mises stress by comparing the stress value with the yield strength, S_y. In this case, S_y = 0.227 Gpa. The critical values of force per unit length, and interference are respectively in:

$$\frac{P_c}{L} = \frac{\pi R (CS_y)^2}{E'} \tag{1}$$

$$\omega_c = R\left(\frac{CS_y}{E}\right)^2 \left[2\ln\left(\frac{2E'}{CS_y}\right) - 1\right] \tag{2}$$

$$C = 1.164 + 2.975\,\nu - 2.906\,\nu^2 \qquad \nu > 0.1938 \tag{3}$$

The value of C is obtained from elasticity considerations, and the critical parameters are obtained at the point of yielding onset, where R and E' are the equivalent radius and equivalent modulus elasticity, respectively.

Sliding is simulated first as a frictionless process, i.e., no coefficient of friction is input in the FE model. Also, repeated sliding is considered, and hence the top cylinder is made to pass over the bottom cylinder just once (i.e., 'one-pass sliding'). Sliding is attained piecewise as the top cylinder traverses a total displacement, Δx (see Fig. 2). This Δx is calculated from geometry and it is a function of the vertical interference, ω, where naturally Δx increases with the preset interference ω. That total distance is divided into n equal load steps, $\delta x = \Delta x/n$. Hence, at load stephasp i the location of the center of the traversing cylinder relative to the center of the stationary cylinder is

$$x = i\delta x - \frac{\Delta x}{2}, \; i = 0, m+n \tag{3}$$

Because of material tugging m load steps are added to ensure exit from sliding contact.

Normalizing x by R, the loading phase is defined by the region $x/R < 0$, where the top cylinder is pressed horizontally against the bottom one before passing the vertical axis of alignment ($x/R = 0$). The unloading phase is defined in the region $x/R > 0$, where the top cylinder has passed the vertical axis of alignment, and where the cylinders are expected to repel each other. As shown in Fig. 1, the nodes at the base of the bottom cylinder are constrained from the displacement in the X and Y direction. The nodes at the base of top cylinder

ISBN : 978-979-3980-15-7
Yogyakarta, 22 November 2008

are also constrained from the displacement in the Y direction, but are allowed to displace freely in the X direction upon sliding.
For this non-linear problem, small load steps are used toward incremental (quasi-static) sliding from one end to the other. Values of the contact force, von Mises stress, and displacement are recorded at each load step. The contact forces are determined by summing the reaction forces at the base of the bottom cylinder.

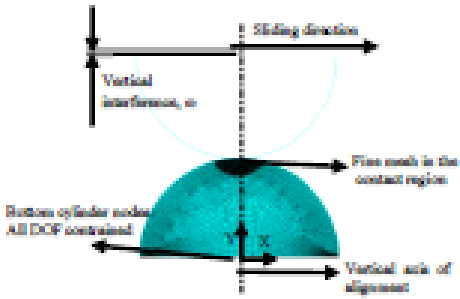

Fig. 1. Schematic of the FEA model for sliding between cylinders

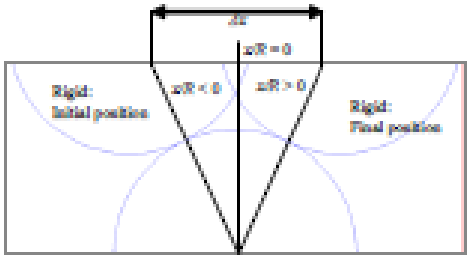

Fig. 2. Schematic of the sliding process

RESULTS AND DISCUSSION

The results are presented for a range of preset normalized vertical interferences, ω^*, from 4 (near the elastic limit) to 40 (elastic-plastic). The material properties used for the cylinders are chosen to be aluminum, which is commonly employed in many engineering application. Convergence of the FE solution is more difficult to achieve for the high vertical interference cases as compared to the lower ones.

Deformation

Since one of cylinders is modeled with a rigid, the deformation pattern that can be observed is only on the bottom cylinder. The displacements of the nodes on the bottom cylinder surface are monitored in order to understand the deformation of the cylinders. The maximum vertical displacement, u_y, is defined as the maximum displacement in the Y direction among the nodes on the contact surfaces of the two cylinders. u_y is effectively normalized by the critical interference ω_c. Sliding is attained piecewise as the top cylinder traverses a total displacement, Δx (see Fig. 2). For the presentation of the results, x is being normalized by the equivalent radius of the cylinders, R, such that $x/R < 0$ signifies loading, and $x/R > 0$ signifies unloading. The cylinders are perfectly aligned at $x/R = 0$. Plots of the normalized vertical displacement, u_y/ω_c , with respect to the normalized sliding distance of the top cylinder, x/R, are presented for the aforementioned of ω^* in Fig. 3.

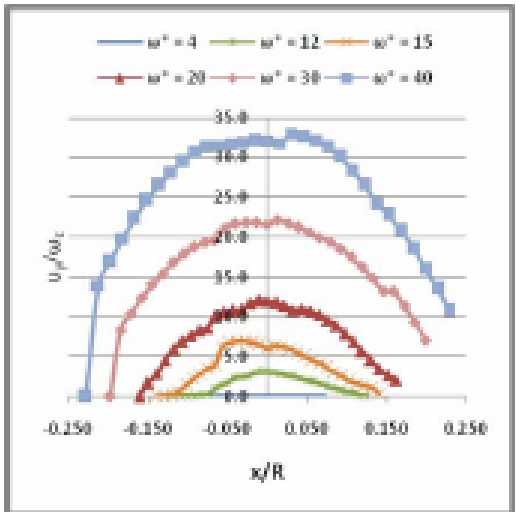

Fig. 3. Normalized maximum vertical displacement vs normalized sliding distance.

For $\omega^* = 4$, the vertical displacement are symmetric about the axis of alignment. Also, displacements increase with the increase in vertical interference ω^*, i.e., with the increase in load. For normal loading, the total maximum vertical displacement is always at the center of contact in bottom cylinder and is equal to the applied vertical interference. However, in sliding contact the location of the points where maximum deformations occurs is found to be at different locations along the sliding direction, i.e., these points are not vertically aligned as in the normal loading case. This explains the magnitude of the vertical deformations being higher than the applied interference. It can be seen that for $\omega^* > 4$, there is plastic deformation where the curves do not come back down to the zero displacement line, i.e., to the X axis.

Forces

Reaction forces at the base nodes of the bottom cylinder are summed for each load step and plotted against the normalized horizontal sliding distance x/R. Both the horizontal reaction force, F_x, and the vertical reaction force, F_y, are normalized by the critical load, P_c. Figure 4 and Figure 5 show the trends followed by F_x/P_c and F_y/P_c respectively, as the top cylinder slides across the bottom one.

For the vertical interference $\omega^* = 4$, the curve is symmetric in Fig. 4 dan Fig. 5, signifying no loss of energy once sliding is completed. For the elastic-plastic loading cases, where $\omega^* > 4$, there are some energy which are lost in the process. This can be seen in Fig. 4 as the area under is larger than the above for all the curves in the elastic-plastic regime..

From Fig. 5 it is also apparent that the normalized vertical reaction force, F_y, is symmetric for all of ω^*. F_y becomes higher as the applied vertical interference is increased.

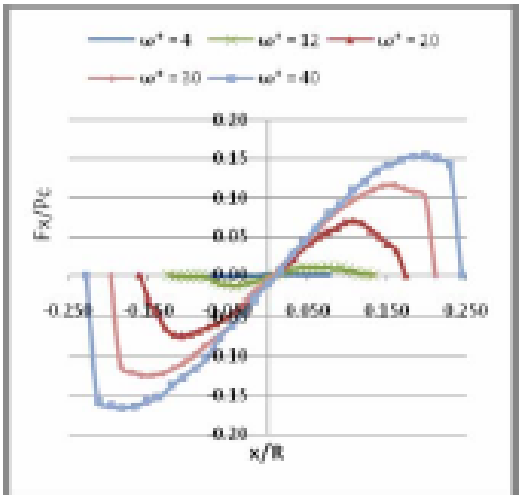

Fig. 4. Normalized horizontal reaction force vs. normalized sliding distance

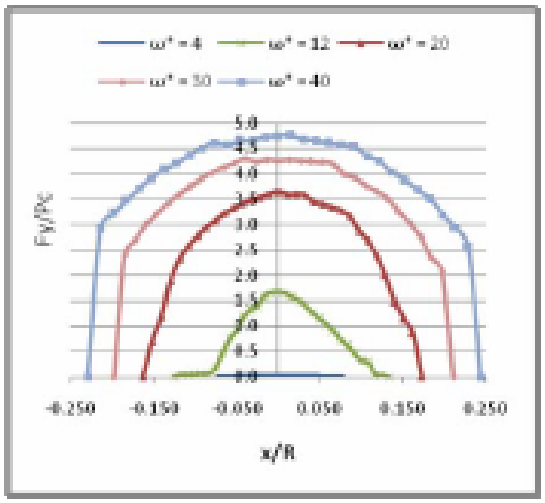

Fig. 5. Normalized vertical reaction force vs. normalized sliding distance

A "load ratio" is defined as F_x/F_y, being the ratio of the horizontal reaction force and the vertical reaction force. This ratio is generated and plotted versus the normalized sliding distance as shown in Fig. 5. This load ratio applies to this isolated mechanical sliding process. It can be seen from Figure 5 that the maximum magnitude of the load ratio increases steadily as ω^* increases. Again, it can be seen that for the plastic loading cases, the ratio of the horizontal to the vertical reaction force is zero at the point where the cylinders are perfectly aligned about the vertical axis.

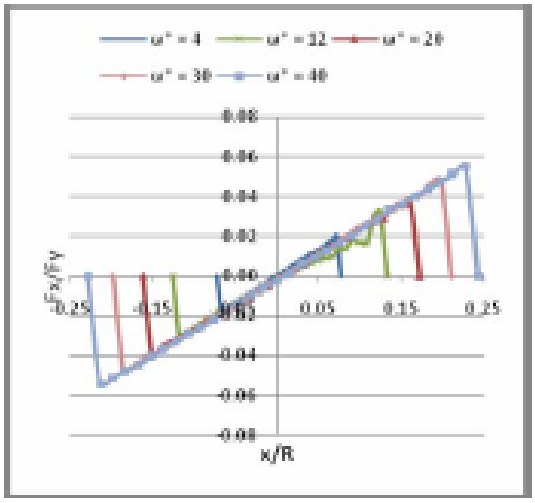

Fig. 6. "Load Ratio" vs. normalized sliding distance

Stress Formations

In this sliding, at low interferences the high stress region develops below the contact interface (see Fig 7). As sliding progresses and load on the cylinder is increases for the elastic-plastic loading ranges, yielding occurs and a sub-surface plastic core develops. Elastic material surrounds this plastic core, and provides the greater part of resistance to sliding.

At the vertical axis of alignment, as seen from Fig. 7, the von Mises stress distribution in the bottom cylinder show regions of slightly higher concentrations in the direction of sliding signifying resistance to sliding. For lower elastic-plastic vertical interferences, such as $\omega^* = 4$, high stresses remain near the area of contact, i.e., there is no significant stress formation at the base of cylinder. As the vertical interferences increase, stresses can be seen developing in the body of the cylinder.

Figure 8 shows the distribution of the residual stresses after sliding is completed for the vertical interferences values of $\omega^* = 4$, and $\omega^* = 40$. As expected, the residual stresses for the case with $\omega^* = 40$ are more widely spread than those for $\omega^* = 4$. Some of these stresses remain at the yield value (i.e., residual plastic strain).

ISBN : 978-979-3980-15-7
Yogyakarta, 22 November 2008

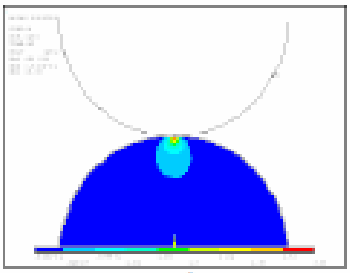

(a) $\omega^* = 4$

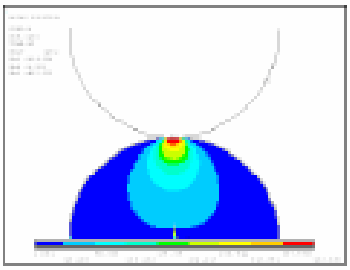

(b) $\omega^* = 40$

Fig 7. von Mises stress contours for sliding cylindrical contact at vertical interferances of (a) $\omega^* = 4$, and (b) $\omega^* = 40$ at the vertical axis of alignment

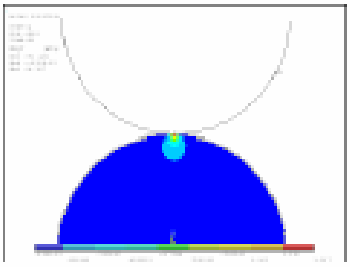

(a) $\omega^* = 4$

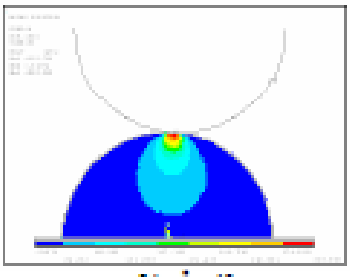

(b) $\omega^* = 40$

Fig 8. Residual von Mises stress contours for sliding cylindrical asperities for (a) $\omega^* = 4$, (b) $\omega^* = 40$

Frictionless vs Frictional Sliding

Figure 9 shows the plot of u_y/ω_i vs x/R for both the frictionless and frictional sliding cases for the vertical interferences of $\omega^* = 15$, 30, and 40. It can be seen from Fig. 9 that magnitude of deformation in the cylinder in frictional sliding is larger than the frictionless sliding. This phenomenon can be also found in the magnitude of the maximum von Mises in every load step.

Figure 10 shows the plot of Maximum von Mises stress vs x/R for both the frictionless and frictional sliding cases for several vertical interferances. It can be seen from Figure 10 that the Maximum von Mises stress in the cylinder in frictional sliding is larger than the frictionless sliding.

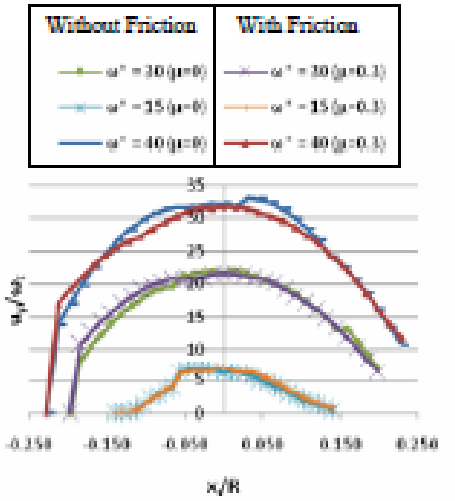

Fig. 9. Comparison of normalized maximum deformation plots in bottom cylinder with and without friction

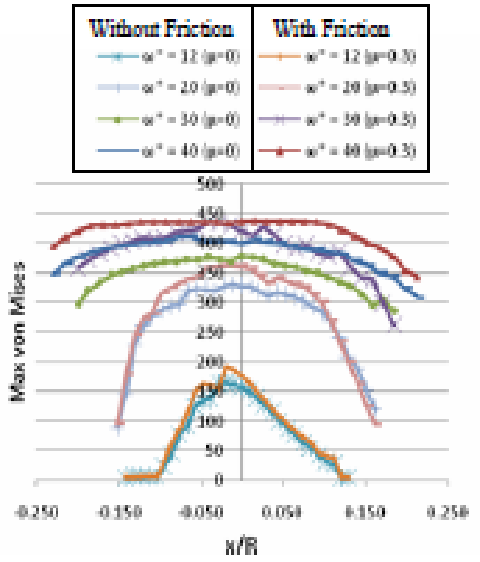

Fig. 10. Comparison of maximum Von Mises stress plots in bottom cylinder with and without friction

CONCLUSIONS

This work presents the results of a FEA of sliding between a rigid cylinder on an elastic-plastic cylinder. Yielding occurs according to the von Mises yield criterion. A 2D plane strain finite element model is utilized to explore the deformations, forces, and stress formations for such frictionless sliding contact. Then a coefficient of friction of magnitude 0.3 is introduced between the two surfaces to simulate frictional sliding.

The maximum deformation at the contact interface increase with the increasing of vertical interference. As sliding progresses into the unloading phase, the deformation curves flatten out at the end to signify permanent plastic deformation at the end of sliding.

The result of the deformation, reaction forces and stress formation of the frictionless sliding contact was compared with the work of Vijaywargiya, et al. [25]. This work performs the similar trend in the deformation and force curve. The advantage of this model is able to reach the higher ω* and less in time consumption in conducting the simulation in ANSYS.

REFERENCES

[1] ASM International Handbook Committee. (1992). ASM Handbook Vol.18: Friction, Lubrication and Wear Technology, USA.

[2] Bayer, R. G. (2004). Mechanical Wear Fundamental and Testing, Marcel Dekker Inc., USA.

[3] Abbot, E.J. and Firestone, F.A. (1933). Specifying Surface Quality — A Method Based on Accurate Measurement and Comparison. Mech. Eng, 55, pp. 569–572.

[4] Greenwood, J.A. and Williamson, J.B.P. (1966). Contact of Nominally Flat Surfaces. Proc. R. Soc. London A 295, pp. 300–319.

[5] Bush, A.W. Gibson, R. D. and Thomas T. R. (1975). The Elastic Contact of Rough Surfaces. Wear, 35, pp. 87-111.

[6] Greenwood, J. A. and Tripp, J. H. (1976). The Elastic Contact of Rough Spheres. ASME Journal of Applied Mechanics, 34. pp. 153-159.

[7] Lo, C.C. (1969). Elastic Contact of Rough Cylinders. Int. J. Mech. Sci, 11, pp. 105-115.

[8] Tsukizoe, T. and Hisakado, T. (1968). On the Mechanism of Contact between Metal Surfaces: Part 2 - The Real Area and the Number of Contact points. ASME Journal of Lubrication Tribology, F90, pp. 81-90.

[9] Whitehouse, D. J. and Archard, J. F. (1970). The Properties of Random Surface of Significance in their Contact. Proceedings of the Royal Society of London, A316, pp. 97-121.

[10] Evseev, D. G. Medvedev, B. M. and Grigoriyan, G. G. (1991). Modification of the Elastic-Plastic Model for the Contact of Rough Surfaces. Wear, 150, pp. 79-88.

[11] Chang, W. R. (1997). An Elastic-Plastic Contact Model for a Rough Surface with an Ion-Plated Soft metallic Coating. Wear, 212, pp. 229-237.

[12] Zhao, Y. W. (2000). An Asperity Microcontact Model Incorporating the Transition from Elastic Deformation to Full Plastic Flow. ASME Journal of Tribology, 122, pp. 86-93.

[13] Jamari, J. (2006). Running-in of Rolling Contacts. PhD Thesis, University of Twente, Enschede, The Netherlands.

[14] Jamari, J. and Schipper, D. J. (2006). An Elastic-Plastic Contact Model of Ellipsoid Bodies. Tribology Letters 21(3), pp. 262-271.

[15] Jamari, J. and Schipper, D. J. (2007). Plastic Deformation and Contact Area of an Elastic-Plastic Contact of Ellipsoid Bodies after Unloading. Tribology International 40(8), pp. 1311-1318.

[16] ANSYS, Inc. (2005). ANSYS Contact Technology Guide. ANSYS, Inc., USA.

[17] Vu-Quoc, L. Zhang, X. and Lesburg, L. (2000). A Normal Force-Displacement Model for Contacting Spheres Accounting for Plastic Deformation: Force-Driven Formulation. ASME Journal of Applied Mechanics, 67, pp. 363-371.

[18] Nosonovsky, M. and Adams, G. G. (2000). Steady-state Frictional Sliding of Two Elastic Bodies with a Wavy Contact Interface. ASME Journal of Tribology, 122(3), pp. 490.

[19] Jackson, R. L. Chusoipin, and Green, I. (2005). A Finite Element Study of the Residual Stress and Deformation in Hemispherical Contacts. ASME Journal of Tribology, 127(3), pp. 484.

[20] Wang, F. and Keer, L. M. (2005). Numerical Simulation for Three Dimensional Elasticplastic

Contact with Hardening Behavior. ASME Journal of Tribology, 2005, 127(3), pp. 494.
[21] Nelias, D. Boucly, V. and Brunet, M. (2005). Elastic-Plastic Contact Between Rough Surfaces: Proposal for a Wear or Running-in Model. ASME Journal of Tribology, 127(3), pp. 494.
[22] Faulkner, A. and Arnell, R. D. (2000). Development of a Finite Element Model to Simulate the Sliding Interaction Between Two, Three-Dimensional, Elastoplastic, Hemispherical Asperities. Wear, 242, pp. 114–122.
[23] Jackson R. L. Duvvuri R. S. Meghani, H. and Mahajan, M. (2007) An Analysis of Elasto-Plastic Sliding Spherical Asperity Interaction. Wear, 262, pp. 210–219.
[24] Moody, J. (2007). A Finite Element Analysis of Elastic-Plastic Sliding of Hemispherical Contacts, Master Thesis, Georgia Institute of Technology, USA.
[25] Vijaywargiya, R. and Green, I. (2006). A Finite Element Study of the Deformation, Forces, Stress Formation, and Energy Loss in Sliding Cylindrical Contacts. International Journal of Non-Linear Mechanics, 42, pp. 914-92.
[26] Green, I. (2005). Poisson Ratio Effects and Critical Values in Spherical and Cylindrical Hertzian Contacts. Int. J. Appl. Mech. 10 (3) pp. 451–462.
[27] Amontons, G., 1699, "On the Resistance Originating in Machines (in French)," Mem. Acad. Roy., pp. 206-222.
[28] Coulomb, C.A., 1785, "The Theory of Simple Machine (in French)," Mem. Acad. Phys. Sci., 10, pp.161-331.
[29] Blau, P. J., 2001, "The significance and use of the friction coefficient," Tribology International, 34, pp. 585–59
[30] Chan, J., Akyuz, U., Xu, L., and Pidaparti, R. M. V., 1998, "Stress Analysis of the Human Temporomandibular Joint," Med. Eng. Phys., 20 [8], pp. 565–572.
[31] Hamilton, G. M., and Goodman, L. E., 1966, "The Stress Field Created by a Circular Sliding Contact," ASME J. Appl. Mech., 33, pp. 371–376.
[32] Hamilton, G. M., 1983, "Explicit Equations for the Stresses beneath a Sliding Spherical Contact," Proc. Inst. Mech. Eng., Part C: Mech. Eng. Sci., 197, pp. 53–59.
[33] Kogut, L., and Etsion, I., 2003, "A Semi-Analytical Solution for Sliding Inception of a Spherical Contact," ASME J. Tribol., 125, pp. 99–506.
[34] Nosonovsky, M., and Adams, G. G., 2000, "Steady-State Frictional Sliding of Two Elastic Bodies with a Wavy Contact Interface," ASME J. Tribol., 122, pp. 490–495.
[35] Boucly, V., Nélias, D., and Green, I., 2007, Modeling of the Rolling and Sliding Contact Between Two Asperities, ASME J. Tribol., 129, pp. 235-245.
[36] ANSYS, Inc., 2005, ANSYS Contact Technology Guide, ANSYS, Inc., USA
[37] Jamari, J., 2006, Running-in of Rolling Contacts, PhD Thesis, University of Twente, Enschede, The Netherlands.
[38] Jamari, J. and Schipper, D.J., 2006, "An Elastic-Plastic Contact Model of Ellipsoid Bodies," Tribology Letters 21(3), pp. 262-271.
[39] Jamari, J. and Schipper, D.J., 2007, "Deformation Due to Contact between a Rough Surface and a Smooth Ball," Wear 262(1-2), pp. 138-145.
[40] Jamari, J. and Schipper, D.J., 2008, "Deterministic Repeated Contact of Rough Surfaces," Wear 264(3-4), pp. 349-358.
[41] Jamari, J. and Schipper, D.J., 2007, "Plastic Deformation and Contact Area of an Elastic-Plastic Contact of Ellipsoid Bodies after Unloading," Tribology International 40(8), pp. 1311-1318.
[42] Jamari, J. and Schipper, D.J., 2006, "Experimental Investigation of Fully Plastic Contact of a Sphere against a Hard Flat," ASME Journal of Tribology 128(2), pp. 230-235